Automated Corneal Nerve Segmentation Using Weighted Local Phase Tensor

Kun Zhao[a,b], Hui Zhang[a*], Yitian Zhao[b,c*], Jianyang Xie[b], Yalin Zheng[c,d], David Borroni[d,f], Hong Qi[e], and Jiang Liu[b,g]

[a]School of Information and Control Engineering, Shenyang Jianzhu University, China.
[b]Ningbo Institute of Industrial Technology, Chinese Academy of Sciences, China.
[c]Department of Eye and Vision Science, University of Liverpool, UK.
[d]St. Paul's Eye Unit, Royal Liverpool University Hospital, UK.
[e]Department of Ophthalmology, Peking University Third Hospital, China.
[f]Department of Ophthalmology, Riga Stradins University, Riga, Latvia.
[g]Department of Computer Science and Engineering, Southern University of Science and Technology, Shenzhen , China
∗Email: yitian.zhao@nimte.ac.cn

Abstract. There has been increasing interest in the analysis of corneal nerve fibers to support examination and diagnosis of many diseases, and for this purpose, automated nerve fiber segmentation is a fundamental step. Existing methods of automated corneal nerve fiber detection continue to pose difficulties due to multiple factors, such as poor contrast and fragmented fibers caused by inaccurate focus. To address these problems, in this paper we propose a novel weighted local phase tensor-based curvilinear structure filtering method. This method not only takes into account local phase features using a quadrature filter to enhance edges and lines, but also utilizes the weighted geometric mean of the blurred and shifted responses to allow better tolerance of curvilinear structures with irregular appearances. To demonstrate its effectiveness, we apply this framework to 1578 corneal confocal microscopy images. The experimental results show that the proposed method outperforms existing state-of-the-art methods in applicability, effectiveness, and accuracy.

Keywords: Corneal nerve, curvilinear structure, segmentation, local phase

1 Introduction

Over the last decade, several studies [1,2,3] have confirmed that numerous corneal nerve properties, such as nerve fiber branching, density, length, tortuosity, etc., are linked to both systemic diseases and conditions of the eye [4,5]. Early detection of these properties may help to reduce the incidence of vision loss and blindness. For this to be possible, accurate detection and analysis of the nerve fiber is essential [6].

In vivo confocal microscopy (IVCM) is the common technique of choice for the imaging and inspection of corneal nerves: in particular, for the non-invasive

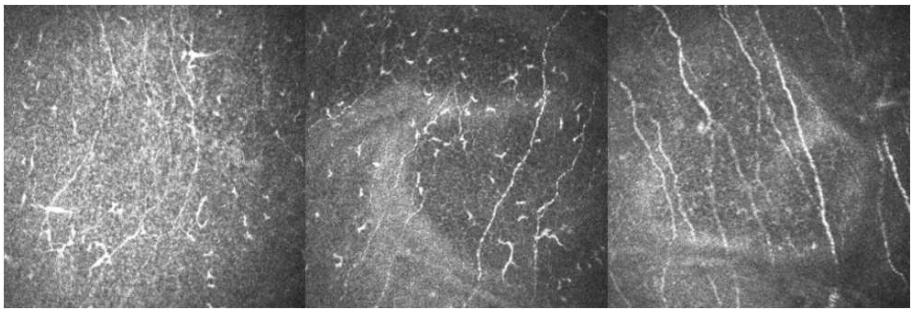

Fig. 1. Corneal nerves images with poor contrast (left), non-target structures (middle), and discontinuous and multiple spatial scales of fibers (right).

acquisition of the subbasal nerve plexus[7]. The manual identification of nerve fiber by ophthalmologists is tedious, highly labour-intensive and subject to human error, while the available commercial software still relies heavily on manual refinement. Consequently, development of an automatic vascular tracing method is indispensable to overcome time constraints and avoid human error.

Extensive work has been carried out on automatic curvilinear structure segmentation (see [8,9] for extensive reviews). Although it bears a superficial similarity to other curvilinear structure segmentation tasks, segmenting corneal nerve fiber is more challenging because of poor contrast and fragmented and multiple scales of tortuous fiber in the image, as shown as Fig. 1. Moreover, many images contain potentially confusing non-target structures such as dendritic cells that can be easily mistaken for fiber given their similar appearance.

In this work, we introduce a new curvilinear feature enhancement metric: namely a weighted local phase tensor. This tensor is enabled by log-Gabor filter, Hessian transform, blurring and shifting functions, to resolve the weak response and discontinuities yielded by most filter-based methods.

1.1 Related Works

Numerous corneal nerve fiber segmentaion methods have been proposed during the last decade. Ruggeri et al. [10] and Scarpa et al. [11] adopted Gabor filtering to enhance nerve visibility: a tracking procedure was then implemented, starting from a set of automatically-defined seed points. Fuzzy c-mean clustering was then applied to classify the pixels as nerve or non-nerve pixels. Poletto [12] further extended the method of [10] to a dataset consisting of 30 epithelium corneal images, the nerves were extracted by connecting the seed points using their minimum cost paths. Dabbah et al. [13] further proposed a multi-scale adaptive dual-model detection algorithm, based on random forest and neural networks.

Ferreira et al. [14] enhanced IVCM images using phase-shift analysis, then identified the nerve structures by using a phase symmetry-based filter. Guimaraes

et al. [15] removed illumination artefacts by applying top-hat filtering and a bank of log-Gabor filters. The hysteresis threshold approach was used to determine the candidate nerve segments, and true and false nerve segments were distinguished using support vector machines (SVM). Annunziata et al. [16] proposed a hand-crafted ridge detector, SCIRD, which utilized curved-support Gaussian models to compute the second order directional derivative in the gradient direction at each pixel. Al-Fahdawi et al. [17] used a coherence filter to improve the IVCM image quality: morphological operations were then applied to remove epithelial cells; the corneal nerves were extracted using an improved edge detection method which was able to bridge the nerve discontinuities. More recently, Colonna et al. [18] used a deep learning approach, the U-Net-based Convolutional Neural Network [19], to trace the corneal nerve. It consisted of a contracting path, which captured nerve descriptors, and a symmetric expanding path, which enabled precise nerve localization.

However, the above-mentioned corneal nerve tracing methods need further improvement, as confocal corneal images contain spurious illumination artefacts, and the whole image may appear dimmed due to focusing problems. Moreover, bright, elongated structures other than nerve segments (e.g., cells), are normally present, and these may cause false-positives. For these reasons, image and nerve enhancement are two essential steps in the process of discriminating the corneal nerve tree.

2 Method

A quadrature filter is a well-designed tool for distinguishing intrinsic features in the image that are invariant to changes in illumination. In this section, we propose the use of a weighted local phase tensor to enhance the fiber structures within the IVCM images.

2.1 Local phase tensor

For a one-dimensional (1D) problem, by using the so-called analytical function, the amplitude $A(x)$ and phase $\phi(x)$ of a given signal $f(x)$ is defined as $A(x) = \|f(x) - if_{\mathcal{H}}(x)\| = \sqrt{f^2(x) + f^2_{\mathcal{H}}(x)}$, and $\phi(x) = \arctan\big(\frac{f(x)}{f_{\mathcal{H}}(x)}\big)$, where $i = \sqrt{-1}$, and $f_{\mathcal{H}}(x)$ is the Hilbert transform of $f(x)$ [20].

In order to enhance spatial localization and to avoid the problems posed by the analytic signal for 2D or higher dimensions and the 2D Hilbert transform, the analysis of the signal must be take over a narrow range of frequencies at different locations in the 2D signal. Boukerroui et al. [20] suggested that local phase should be estimated by a quadrature filter with even-symmetric and odd-symmetric parts. In consequence, the definition of local phase in 2D application may be rewritten as:

$$\phi(x) = \arctan\Big(\frac{f_e(x) * f(x)}{f_o(x) * f(x)}\Big) = \arctan\Big(\frac{E(x)}{O(x)}\Big). \tag{1}$$

where $f_e(x) * f(x)$ is the even (symmetric) band-pass filter and denotes as $E(x)$, while $f_o(x) = \mathcal{H}(f_e(x))$ is the Hilbert transform of the even filter $f_e(x)$, and denotes as $O(x)$. In particular, the log-Gabor (log normal) filter is a commonly used quadrature filter, and $E(x)$ and $O(x)$ are the responses of even and odd quadrature pair filter to an image can be estimated by:

$$E(x) = \text{real}\{F^{-1}(\text{LG}(\omega) \times F(x))\}, \tag{2}$$

$$O(x) = \text{imag}\{F^{-1}(\text{LG}(\omega) \times F(x))\}, \tag{3}$$

where LG, F and F^{-1} indicate the log-Gabor filtering, the forward and inverse Fourier transforms, respectively.

Then the local phase tensor in symmetric and asymmetric aspects $\mathcal{T}_E$ and $\mathcal{T}_O$ are calculated as [21]:

$$\mathcal{T}_E = [\mathbf{H}(E(x))] \cdot [\mathbf{H}(E(x))]^T, \tag{4}$$

$$\begin{aligned} \mathcal{T}_O = &-\frac{1}{2}([\nabla(O(x))] \cdot [\nabla\nabla^2(O(x))]^T \\ &+ [\nabla\nabla^2(O(x))] \cdot [\nabla(O(x))]^T), \end{aligned} \tag{5}$$

where $\mathbf{H}$ denotes the Hessian operation, and ∇, ∇^2 indicates the Gradient and Laplacian operations, respectively. The superscript T denotes the transpose operation.

According to the monogenic signal analysis [22], the local phase tensor can be obtained by:

$$\mathcal{T} = \sum_{\theta=1}^{\Theta} \left\{ \sqrt{(\mathcal{T}_E^\theta)^2 + (\mathcal{T}_O^\theta)^2} \right\} \cdot \cos(\varphi). \tag{6}$$

In practice, multiple orientations are needed to capture structures at different directions. Furthermore, in order to achieve a rationally invariant tensor, filters for all directions have to be combined. Θ indicates the set of directions under consideration: $\Theta = \{\frac{\pi}{16}, \frac{2\pi}{16}, \frac{3\pi}{16}, \cdots, \frac{15\pi}{16}, \pi\}$. The instantaneous phase φ presenting the local contrast independently of feature type (line and edge), and may be defined as

$$\varphi(x) = E^\theta(x) + |O^\theta(x)|i, \tag{7}$$

As observed from Eqn. (2) and Eqn. (3), $E(x)$ reaches the maximal response at lines while $O(x)$ is almost 0, the filter response is purely real, and leads to a line-like signal. While for edges, the $E(x)$ is 0 and $O(x)$ has the maximal response, and the filter response is purely imaginary. This suggests that image edges align with the zero crossing of the real part of the phase map. Therefore, the real part of the response $E^\theta(x)$ and the absolute value of the imaginary part $O^\theta(x)$ are used, with a view to avoid confusion caused by changes in structural direction.

2.2 Weighted local phase tensor

In real applications, due to poor contrast the extracted responses of the corneal nerves are represented as discontinuities. In consequence, in order to permit greater tolerance of the positions, deformations and scales of the respective contours, blurring and shifting operations are applied to the local phase tensor. The blurring operation is able to suppress the noise or background, and the shifting operation is used to enhance the response of the quadrature filter by maximizing all neighboring pixels in low-contrast in the dark and low contrast regions [23].

The blurring consists of a dilation of the filter response with a Gaussian function G_σ with standard deviation σ: $\sigma = \sigma_0 + \alpha\rho$. The σ_0 and α are the constants that regulate the tolerance to deformation of the concerned responses, and ρ is the radius parameter, representing a linear function of the distance from the centre of the quadrature filter. We then shift each blurred local phase tensor by a distance ρ_i in the direction opposite to ϕ_i. Formally, the i-th blurred and shifted responses $S_{\sigma_i,\rho_i,\phi_i}$ of the local phase tensor $\mathcal{T}$ can be calculated by:

$$\begin{aligned} &S_{\rho_i,\phi_i}(u,v) = \\ &\max_{u',v'}\{\mathcal{T}_{\sigma_i}(u-\Delta u_i-u', v-\Delta v_i-v')G_{\sigma'}(u',v')\}. \end{aligned} \tag{8}$$

where $-3\sigma \leq u',\ v' \leq -3\sigma$. The above configuration process represents a convolution of the weighting function with respect to the filter center u, v, and $S = \{(\rho_i, \phi_i)|i = 1, \ldots, n\}$, where n indicates the number of quadrature responses. $\Delta u_i = -\rho_i \cos\phi_i$ and $\Delta v_i = -\rho_i \sin\phi_i$ is the shift vector of i-th quadrature responses in Cartesian coordinates. This shift operation is able to assemble all the responses at the proposed filter centre. The parameter values of S can be automatically determined from the aforementioned filter settings of the standard deviation of the filter responses, kernel size, and orientations: $\rho_i \in \{0, 2, 4\}$ and $\phi_i \in \{0, 0.5\pi, \pi, 1.5\pi\}$.

Then the weighted local phase tensor $\hat{\mathcal{T}}$ for a given image is defined as a threshold ϵ of a multiplication of S_{ρ_i,ϕ_i}:

$$\hat{\mathcal{T}} = \left| \prod_{i=1}^{|S|} (S_{\rho_i,\phi_i}) \right|^{\epsilon}. \tag{9}$$

where ϵ denotes the control parameter that sets the threshold of the response at a fraction ϵ $(0 \leq \tau \leq 1)$ of the maximum response.

In order to enhance curvilinear structures of different sizes present within a single image, multiple scales fusion is needed. In our study, the given image is uniformly down-sampled to $1/m$ of its original size, and the fused local phase tensor is defined as:

$$\hat{\mathcal{T}} = \frac{\sum_{m=1}^{M} \mathcal{T}_m |\mathcal{T}_m|^\gamma}{\sum_{m=1}^{M} |\mathcal{T}_m|^\gamma} \tag{10}$$

where $m \in \{1, \cdots M\}$, and M denotes the number of scales ($M = 3$ in this work). γ is the order number of the power of the magnitude of the filter response at

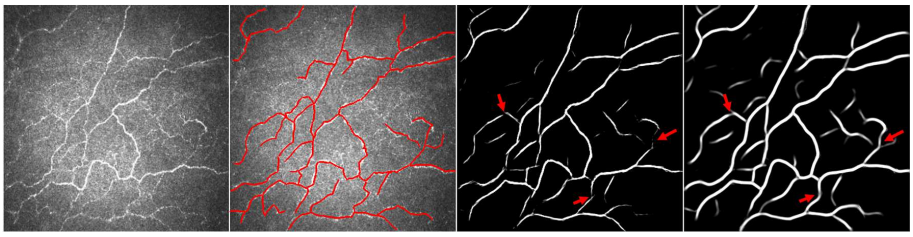

Fig. 2. Illustrative enhancement results using the local phase tensor and weight local phase tensor. (a) original image; (b) groundtruth; (c) response of local phase tensor; (d) response of weighted local phase tensor.

each scale. Fig. 2 demonstrates that the proposed weighted local phase tensor acts as a general curvilinear structure indicator, providing an improved local phase tensor. It may be observed that the proposed weighted local phase tensor is able to better preserve poorly-imaged, low-contrast fibers, which appear as discontinuous to the unweighted tensor (Fig. 2(c) and (d): red arrows).

3 Materials and Evaluation metrics

3.1 Dataset

A total of 1578 images of corneal subbasal epithelium from 108 normal and pathological subjects were acquired using a Heidelberg Retina Tomograph equipped with a Rostock Cornea Module (HRT-III) microscope (Heidelberg Engineering Inc.). The 108 subjects included: 30 healthy subjects; 18 subjects with diabetes; and 60 subjects with dry eye disease. The image resolution was 384×384 pixels, and the field of view was $400 \times 400 \mu m^2$. The nerves appear as bright curvilinear structures lying over a darker background. The reference groundtruth was segmented manually by an ophthalmologist, who traced the centerlines of all visible nerves using an in-house program written in Matlab (Mathworks R2017, Natwick).

3.2 Evaluation metrics

To compare the nerve fiber tracing performance of the proposed method with the corresponding groundtruth, we computed the *sensitivity* and *false discovery rate* (FDR) [15] between the predicted centerlines and groundtruth centerlines. Sensitivity is the fraction of the number of pixels in the correctly detected nerve segments (true positives) nerves over the total number of pixels in the groundtruth nerves. FDR is defined as the fraction of the total number of pixels incorrectly detected as nerve segments(false positives) nerves over the total number of pixels of the traced nerves in groundtruth. The use of *specificity*, defined as the number of pixels correctly rejected as non-nerve structures (true negatives), is

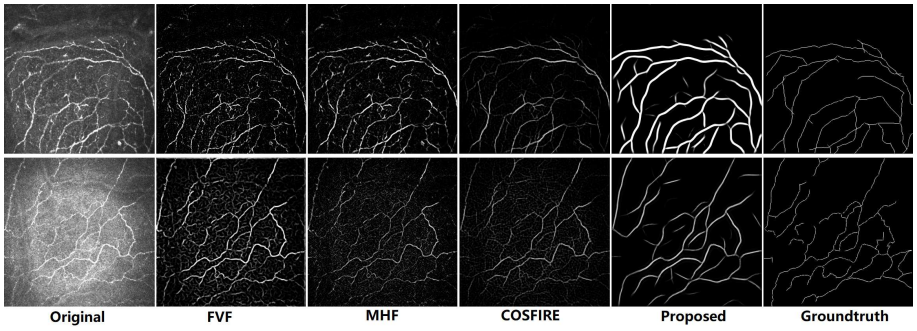

Fig. 3. Illustrative results of corneal nerve filtered by different curvilinear structure enhancement methods.

not adequate for the evaluation of this tracing task, since the vast majority of pixels do not belong to corneal nerves.

It is worth noting that, as is customary in the evaluation of methods extracting one pixel-wide curves [15], a three-pixel tolerance region around the manually traced nerves is considered to be a true positive. In other words, a predicted centerline point is considered as true positive if is no more than three pixels distant from the nearest ground truth centerline point.

4 Experimental Results

We validated the effectiveness of the proposed weighted local phase tensor-based nerve fiber segmentation method against three other state-of-the-art curvilinear structure enhancement methods: Frangi's Vesselness filter (FVF) [24], multiscale hessian filter (MHF) [25], and combination of shifted filter responses (COSFIRE) [23]. An infinite perimeter active contour with hybrid region (IPACHR) method [26] is used to segment the fibers from the filtered curvilinear structures. However, other sophisticated segmentation methods may work equally well. For a fair comparison, the parameters of these filters were optimized for best performance as follows. **FVF** scales: 1-8, scale ratio: 2; **MHF** scales: 1-3, spacing resolution: [3;3]; **COSFIRE** scales: 1-4, orientation: $\theta \in \{\frac{\pi i}{8} | i = 0, \cdots 7\}$, threshold value: 0.35.

Fig. 3 demonstrates the filtered curvilinear structures obtained by applying these different methods. Overall, all methods demonstrated similar performance on fibers with large diameters. It can be seen that FVF is able to enhance most larger fibers, but falsely enlarges background features where intensity inhomogeneities are present. MHF misses most fibers with small diameters, and also enhances some background regions, which leads to inaccurate identification of the fiber structures. As for the COSFIRE, the fiber edges are clearly enhanced, and this method achieves better results in distinguishing fiber from background. However, the COSFIRE also enhanced some surrounding non-target structures.

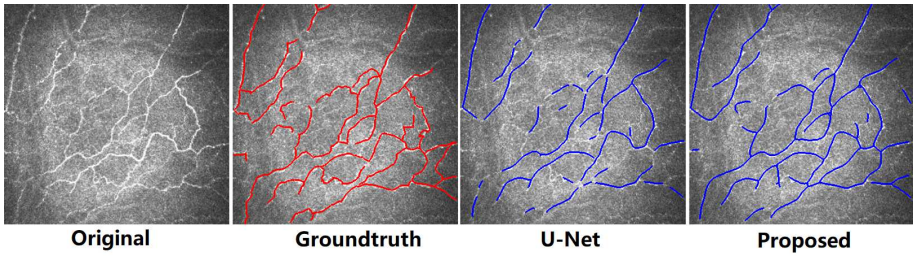

Fig. 4. Illustrative results of corneal nerves traced by U-Net and by the proposed method.

Table 1. Performance of five different segmentation methods.

Methods	Sensitivity	FDR
FVF	0.912 ± 0.25	0.181 ± 0.12
MHF	0.933 ± 0.19	0.142 ± 0.11
COSFIRE	0.950 ± 0.24	0.113 ± 0.09
U-Net	0.956 ± 0.17	0.105 ± 0.08
Proposed	**0.963 ± 0.12**	**0.096 ± 0.09**

In contrast to these filters, we can see that the proposed method generally demonstrated superior performance in detecting nerve fiber regions (uniform responses at both high and low intensities), and provided relatively stronger responses to small fibers than other methods. In other words, the proposed method is not only able to enhance fiber regions so as to stand out more conspicuously from background, but also has the ability to reject non-fiber features. Such properties are due to the proposed filter retaining the intrinsic information of features that are invariant to changes in intensity, location and scale, which permits better detection of curvilinear structures under varying conditions. Table 1 shows this superior segmentation performance based on the proposed curvilinear structures enhancement method, demonstrating both higher sensitivity and lower FDR by significant margins.

It is interesting to note that the visual results (Fig. 4) and evaluation metrics (Table 1) demonstrate that our method performs better than the deep learning-based approach: U-Net [19], which has recently attracted attention. We employed the U-Net-based convolutional neural network [18] for the fully automatic segmentation of corneal nerves from the IVCM image. This network comprises a contracting-encoder and an expanding-decoder, which allows the user to obtain a label classification for every single pixel. We trained the U-Net on randomly sampled images from the database, reserving 20% of this database as a validation set.

5 Conclusions

Nerve fiber segmentation is the fundamental step in automated diagnosis of many nerve-related diseases, and it remains a challenging medical image analysis problem despite considerable effort in research. Many factors come together to make this problem difficult to address, such as uneven illumination and noise in the original image. In this paper, we have presented a weighted local phase tensor-based curvilinear structure filtering method, and have applied it successfully to corneal nerve fiber segmentation. The proposed filter exploits the advantages of a local phase tensor, making use of the geometric mean of blurred and shifted quadrature filter responses to allow more tolerance in the position of the respective contours. The evaluation results demonstrate the superiority of our model when compared with other state-of-the-art methods. It is our intention in our future work to measure the tortuosity, length, and density of the extracted nerves, so as to further evaluate the significance of changes in these morphological features and their association with nerve-related diseases, such as diabetic neuropathy.

6 Acknowledgment

This work was supported by National Natural Science Foundation of China (61601029, 61602322), Zhejiang Provincial and Ningbo Natural Science Foundation (LZ19F010001, 2018A610055).

References

1. R. Annunziata, A. Kheirkhah, S. Aggarwal, P. Hamrah, and E. Trucco. A fully automated tortuosity quantification system with application to corneal nerve fibres in confocal microscopy images. *Med. Image Anal.*, 32:216–232, 2016.
2. K. Edwards, N. Pritchard, D. Vagenas, A. W. Russell, R. A. Malik, and N. Efron. Standardizing corneal nerve fibre length for nerve tortuosity increases its association with measures of diabetic neuropathy. *Diabetic medicine : a journal of the British Diabetic Association*, 31 10:1205–9, 2014.
3. J. Kim and M. Markoulli. Automatic analysis of corneal nerves imaged using in vivo confocal microscopy. *Clin. Exp. Optom.*, 101 2:147–161, 2018.
4. Yitian Zhao, Yalin Zheng, Yifan Zhao, Yonghuai Liu, Zhili Chen, Peng Liu, and Jiang Liu. Uniqueness-driven saliency analysis for automated lesion detection with applications to retinal diseases. In *Medical Image Computing and Computer Assisted Intervention - MICCAI 2018 - 21st International Conference, Granada, Spain, September 16-20, 2018, Proceedings, Part II*, pages 109–118, 2018.
5. Yitian Zhao, Jianyang Xie, Pan Su, Yalin Zheng, Yonghuai Liu, Jun Cheng, and Jiang Liu. Retinal artery and vein classification via dominant sets clustering-based vascular topology estimation. In *Medical Image Computing and Computer Assisted Intervention - MICCAI 2018 - 21st International Conference, Granada, Spain, September 16-20, 2018, Proceedings, Part II*, pages 56–64, 2018.

6. Yitian Zhao, Jingliang Zhao, Jian Yang, Yonghuai Liu, Yifan Zhao, Yalin Zheng, Likun Xia, and Yongtian Wang. Saliency driven vasculature segmentation with infinite perimeter active contour model. *Neurocomputing*, 259:201–209, 2017.
7. F. Scarpa, X. Zheng, Y. Ohashi, and A. Ruggeri. Automatic evaluation of corneal nerve tortuosity in images from in vivo confocal microscopy. *Invest. Ophth. Vis. Sci.*, 52 9:6404–8, 2011.
8. M. Fraz, P. Remagnino, A. Hoppe, B. Uyyanonvara, A. R. Rudnicka, C. G. Owen, and S. A. Barman. Blood vessel segmentation methodologies in retinal images - a survey. *Comput. Meth. Prog. Bio.*, 108:407–433, 2012.
9. Y. Zhao, Y. Zheng, Y. Liu, Na, and Y. Wang J. Liu. Automatic 2d/3d vessel enhancement in multiple modality images using a weighted symmetry filter. *IEEE Trans. Med. Imaging*, 37(2):438–450, 2018.
10. A. Ruggeri, F. Scarpa, and E. Grisan. Analysis of corneal images for the recognition of nerve structures. *2006 International Conference of the IEEE Engineering in Medicine and Biology Society*, pages 4739–4742, 2006.
11. F. Scarpa, E. Grisan, and A. Ruggeri. Automatic recognition of corneal nerve structures in images from confocal microscopy. *Invest. Ophth. Vis. Sci.*, 49 11:4801–7, 2008.
12. E. Poletti and A. Ruggeri. Automatic nerve tracking in confocal images of corneal subbasal epithelium. In *Proceedings of the 26th IEEE International Symposium on Computer-Based Medical Systems*, pages 119–124, 2013.
13. M. A. Dabbah, J. Graham, I. N. Petropoulos, M. Tavakoli, and R. A. Malik. Automatic analysis of diabetic peripheral neuropathy using multi-scale quantitative morphology of nerve fibres in corneal confocal microscopy imaging. *Med. Image Anal.*, 15(5):738–747, 2011.
14. A. Ferreira, A. Morgado, and J. Silva. A method for corneal nerves automatic segmentation and morphometric analysis. *Comput. Meth. Prog. Bio.*, 107 1:53–60, 2012.
15. P. Guimarães, J. Wigdahl, and A. Ruggeri. A fast and efficient technique for the automatic tracing of corneal nerves in confocal microscopy. In *Transl. Vis. Sci. Techn.*, 2016.
16. R. Annunziata, A. Kheirkhah, P. Hamrah, and E. Trucco. Boosting hand-crafted features for curvilinear structure segmentation by learning context filters. In *Medical Image Computing and Computer-Assisted Intervention - MICCAI 2015*, pages 596–603, 2015.
17. S. Al-Fahdawi, R. Qahwaji, A. S. Al-Waisy, S. S. Ipson, R. A. Malik, A. Brahma, and X. Chen. A fully automatic nerve segmentation and morphometric parameter quantification system for early diagnosis of diabetic neuropathy in corneal images. *Comput. Meth. Prog. Bio.*, 135:151–166, 2016.
18. A. Colonna, F. Scarpa, and A. Ruggeri. Segmentation of corneal nerves using a u-net-based convolutional neural network. In *MICCAI 2018 workshop OMIA*, pages 185–192, 2018.
19. Olaf Ronneberger, Philipp Fischer, and Thomas Brox. U-net: Convolutional networks for biomedical image segmentation. In *Medical Image Computing and Computer-Assisted Intervention - MICCAI 2015*, pages 234–241, 2015.
20. D. Boukerroui, J. Noble, and M. Brady. On the choice of band-pass quadrature filters. *J. Math. Imaging Vis.*, 21:53–80, 2004.
21. I. Hacihaliloglu, A. Rasoulian, P. Abolmaesumi, and R. Rohling. Local phase tensor features for 3d ultrasound to statistical shape+pose spine model registration. *IEEE Trans. Med. Imaging*, 33:2167–2179, 2014.

22. M. Felsberg and G. Sommer. The monogenic signal. *IEEE Trans. Signal Process.*, 49:3136–3144, 2001.
23. G. Azzopardi, N. Strisciuglio, M. Vento, and N. Petkov. Trainable COSFIRE filters for vessel delineation with application to retinal images. *Med. Image Anal.*, 19:46–57, 2015.
24. Alejandro F. Frangi, Wiro J. Niessen, Koen L. Vincken, and Max Viergever Viergever. Multiscale vessel enhancement filtering. In *Med. Image Comput. Comput. Assist. Interv.*, volume 1496, pages 130–137, 1998.
25. T. Jerman, F. Penus, B. Likar, and Z. Spiclin. Enhancement of vascular structures in 3D and 2D angiographic images. *IEEE Trans. Med. Imaging*, 35(9):2107–2118, 2016.
26. Y. Zhao, L. Rada, K. Chen, and Y. Zheng. Automated vessel segmentation using infinite perimeter active contour model with hybrid region information with application to retinal images. *IEEE Trans. Med. Imaging*, 34(9):1797–1807, 2015.